A scalable, fast, and multichannel arbitrary waveform generator

M. T. Baig, M. Johanning, A. Wiese, S. Heidbrink, M. Ziolkowski, and C. Wunderlich

Re-register for Table of Content Alerts

Create a profile.   Sign up today!

A scalable, fast, and multichannel arbitrary waveform generator

M. T. Baig, M. Johanning, A. Wiese, S. Heidbrink, M. Ziolkowski, and C. Wunderlich[a]

Department of Physics, University of Siegen, Walter-Flex-Strasse 3, Siegen NRW 57072, Germany

This article reports on the development of a multichannel arbitrary waveform generator that simultaneously generates arbitrary voltage waveforms on 24 independent channels with a dynamic update rate of up to 25 Msps. A real-time execution of a single waveform and/or sequence of multiple waveforms in succession, with a user programmable arbitrary sequence order is provided under the control of a stand-alone sequencer circuit implemented using a field programmable gate array. The device is operated using an internal clock and can be synced to other devices by means of transistor-transistor logic (TTL) pulses. The device can provide up to 24 independent voltages in the range of up to ± 9 V with a dynamic update-rate of up to 25 Msps and a power consumption of less than 35 W. Every channel can be programmed for 16 independent arbitrary waveforms that can be accessed during run time with a minimum switching delay of 160 ns. The device has a low-noise of 250 μV_{rms} and provides a stable long-term operation with a drift rate below 10 μV/min and a maximum deviation less than ± 300 μV_{pp} over a period of 2 h. © 2013 AIP Publishing LLC. [http://dx.doi.org/10.1063/1.4832042]

I. MOTIVATION

Ion traps have promising potential in the field of quantum information science,[1–4] and in particular micro-structured Paul traps are well suited for this purpose. They can have multiple zones for trapping, processing, and storing of atomic ions.[5–9] Scaling such traps up for quantum information processing requires a large number of independent high bandwidth, low noise voltage signals.

In this approach, a register of quantum bits (qubits) is stored in the internal states of laser-cooled trapped ions (forming a Wigner crystal), and in some implementations in motional states of their normal modes.[1] Wigner crystals of increasing length become difficult to cool and to protect against environmental influences and thus are subject to decoherence. This is detrimental for tasks that rely on the computational power of quantum superpositions and entanglement. Splitting the quantum register into crystals of manageable size and entangling them on demand in a quantum network is regarded as a promising and straight-forward solution. This can be achieved in segmented ion traps where storage, shuttling, and processing zones[5, 10] are realized by a large number of DC electrodes. These type of traps are often regarded as a prerequisite to scalable quantum information processing using trapped ions.

Specific implementations of such a partitioned quantum register require shuttling of ions in order to be able to exchange information between independent crystals and this is ideally done with low heating of the motional state.[10] This can be achieved by shuttling of the ions in an adiabatic fashion, at the expense of long shuttling times,[11] or in an tailored diabatic way which can be optimized for low heating.[6, 12, 13] The latter requires voltages with a fast update rate.

Another building block of this type of quantum information processing is splitting and merging strings of ions, again

requiring precise control over a large number of voltages.[14] Various proposals for processing quantum information exist, among others the network model,[15, 16] or measurement based quantum computation,[17] relying on highly entangled graph states, which could be generated in ion traps.[18]

Shuttling and the tailoring of interactions cannot only be done by manipulating the DC voltage, but also the RF voltage used for radial trapping of an ion string.[19] A general purpose quantum processor would be a field programmable trap array (FPTA). Independent arbitrary time-dependent potentials (e.g., sums of dc and rf voltages) can be applied to each element of the FPTA, allowing for the creation of arbitrary trapping potentials (compared to designs optimized for a fixed lattice[20]) and the investigation of various lattice types and quantum simulations thereof with a single programmable trap (a similar concept is discussed in Ref. 21). For certain types of ions and trap sizes, the device presented here already fulfills all the necessary requirements. This type of application might require – depending on the selected ion and trap design – higher amplitudes or update rates than supplied by the device described here, and, to reduce heating, narrow band filtering of the RF component.

Similarly, quantum simulators require a high degree of control to simulate the features of other quantum systems.[3, 4, 22] The interaction between trapped ions could be tailored to mimic an entirely different quantum system, for example, by shaping the axial trapping potential.[23, 24] This application, too, requires a large number of independent voltages.

Furthermore, in the field of experimental quantum optics, laser fields are often used to manipulate the internal or motional state of atoms, and need to be shaped in time and space. Shaping the temporal profile of laser pulses can be realized using acousto-optic modulators (AOMs), where control signals can be used to generate arbitrary amplitude and frequency patterns of a laser.[25, 26] The spatial profile of a laser beam can be manipulated by a spatial light modulator (SLM),

[a] Electronic mail: wunderlich@physik.uni-siegen.de

typically implemented as a liquid crystal display (LCD) or digital micro-mirror devices. The SLMs often take digital signals for control using pulse width modulation, but analog implementations exist[27] potentially requiring again a large set of independent voltages. In the same fashion, the spectral and accordingly temporal profile of large bandwidth lasers and frequency combs can be manipulated.[28] Other applications in the quantum optics community, for example, the generation of control signals to shape magnetic or dipole traps for neutral atoms[29, 30] and using SLMs for wave front sensing, adaptive imaging, and holography also require a large number of individual voltages.

Commercially available devices do not meet the requirements of precise enough voltages combined with a fast update rate as needed for quantum optics experiments. This article reports on the design, development, and characterization of a scalable, fast, and multichannel arbitrary waveform generator (MAWG)[31] that meets the requirements of advanced quantum optics experiments.

II. HARDWARE ARCHITECTURE

A general architecture of the device is shown in Fig. 1. The MAWG consists of a control-board interfacing with 12 identical daughter-cards via a backplane. The control-board receives the waveform-data as well as control instructions from a control computer via a USB 2.0 interface. A field programmable gate array (FPGA) on the control-board decodes the control instructions and stores the provided waveform-data on the memory of a desired daughter-card or retrieves the pre-stored waveform-data from the memory of the daughter-card according to the control instruction. The backplane provides distribution of signals and voltage supplies to all of the daughter-cards. Each daughter-card has two channels to generate two independent voltages which are individually terminated and low-pass filtered on a remote termination-board resulting in the final voltage signals to be used in the desired application. A dedicated synchronous dual-port static RAM
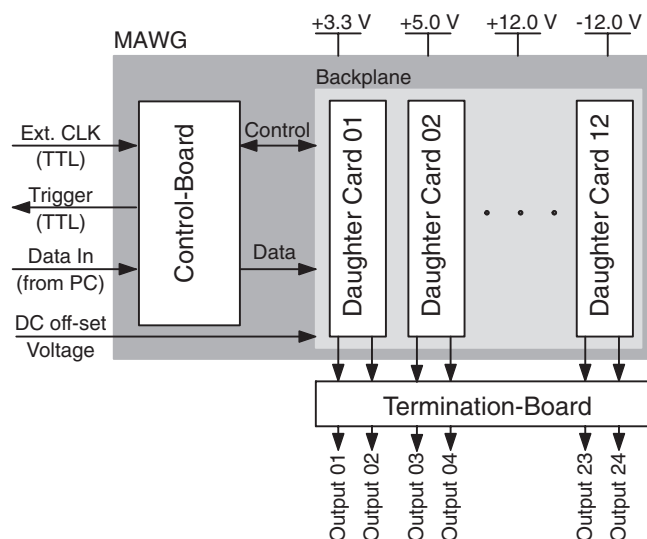
TABLE I. List of main components used in the MAWG.

Component	Company	Part #
USB μC	Cypress Semiconductor	CY7C68013A
FPGA	Xilinx, Inc.	XC3S500E
Serial EEPROM	Microchip Technology	24LC64
CPROM	Xilinx, Inc.	XCF04S
Crystal	Vishay	XT49M
Oscillator	IQD Frequency Products Limited	IQXO-22C
CPLD	Lattice Semiconductor	ISPMACH4064V
DP-SRAM	Integrated Device Technology	70V3599
Voltage Reference	Maxim Integrated	MAX6161
DAC	Maxim Integrated	MAX5885
OP-AMP	Analog Devices	AD8021AR
Digital Isolator A	Analog Devices	ADUM1100BRZ
Digital Isolator B	Analog Devices	ADUM1401CRWZ
Octal Bus Transceiver	Texas Instruments	SN74LVT245B
DC-DC Converter	Texas Instruments	TPS54610PWP

(DP-SRAM) is provided to each of the daughter cards to store waveforms data for every channel individually up to 128 k depth. A complex programmable logic device (CPLD) on every daughter card controls the flow of the data and the clock to both of the channels locally. The general architecture of the MAWG with flow of data signals among main parts of the device is shown in Fig. 1.

The MAWG is optimized to get a good quality signal (in terms of low reflections, drift, and noise) for operations up to an update rate of 25 Msps. A user defined internal clock, provided by the FPGA on the control board, or an external transistor-transistor logic (TTL) signal can be used to operate the device in an *asynchronous* or *synchronous* mode of operation, respectively. In addition, a TTL pulse signal is provided by the MAWG device to trigger the operations of other devices in the experiment. The user-defined voltage waveforms can optionally be shifted by a DC off-set voltage.

The updating of waveforms in the device memory – the *write* operation – is done sequentially, channel-by-channel with one channel at once, while the actual generation of voltages – the *read* operation – is executed simultaneously and synchronously for all of the 24 channels. Provision of the dedicated memory for each channel and simultaneous read for all channels correspond to a digital bandwidth of 9.6 Gbps.

A list of the main integrated circuit components (ICs) used for the MAWG device is provided in Table I.[32] All components were chosen to satisfy various assessment criteria, importantly, high dynamic range of speed and amplitude, supportive contribution to low-noise and environmental stable performance, as well as possibly general simplicity and high reliability at the same time.

FIG. 1. The general architecture of the MAWG showing the inputs, the outputs and flow of data and control signals among main parts of the device.

A. The control board

The control-board holds both fixed- and firmware-type circuitry, which are primarily needed to receive user-defined waveform and/or control instructions sent from the control
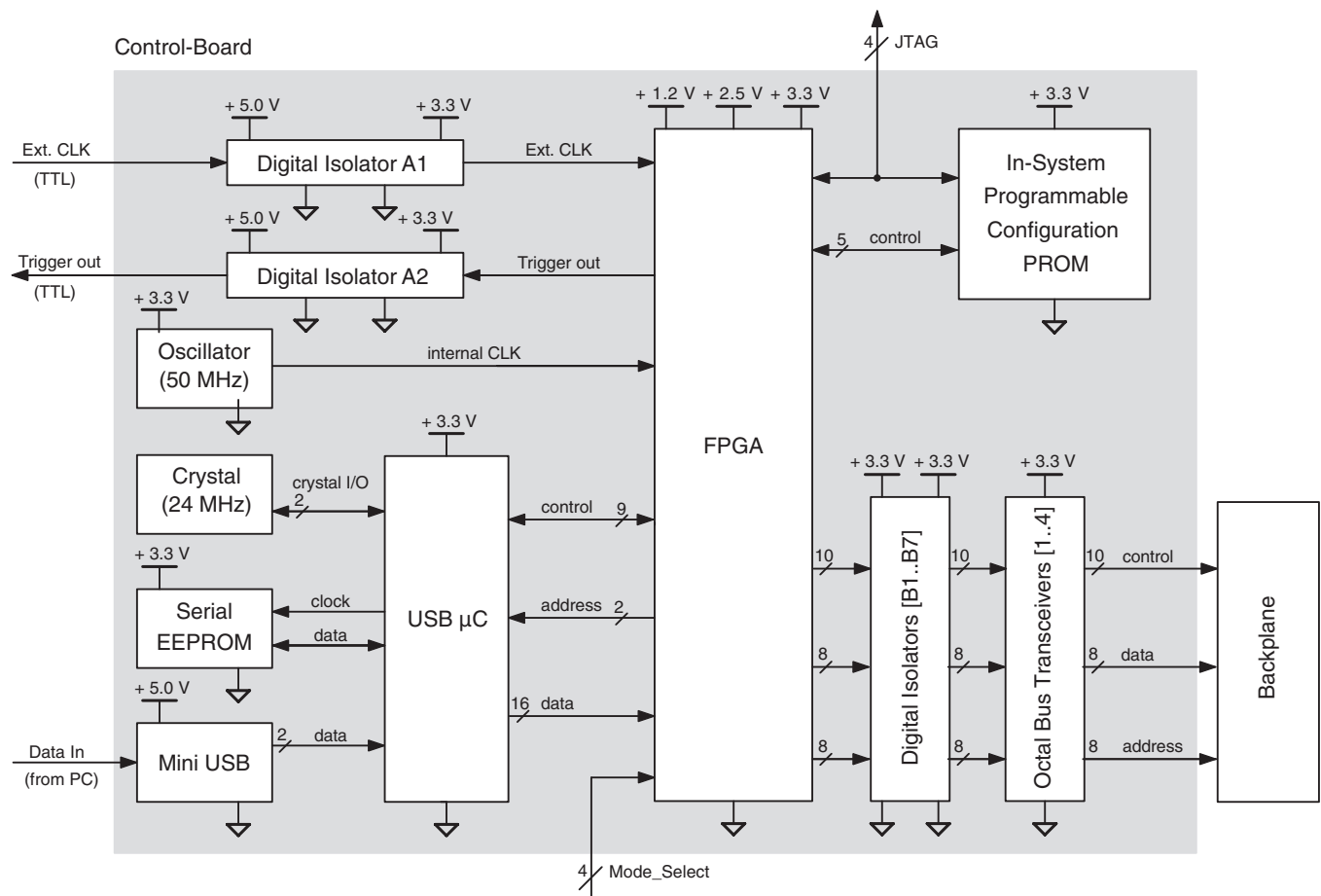
FIG. 2. Data and signal flow among the components on the control-board. The USB μC receives the data from the control computer via the USB and transfers it to the FPGA which delivers the data to the backplane through the digital isolators and the octal bus transceivers. An optional TTL input and a TTL output are also provided through the digital isolators. The CPROM and the EEPROM are provided to auto-configure the FPGA and the USB μC, respectively.

computer, and furthermore to process and to deliver them to the daughter-cards through the backplane in a controlled way.

The data are received from the control computer by the USB micro-controller (μC) via the USB interface and delivered to the FPGA in a 2-bytes word format. The FPGA analyses the data and delivers a single-byte-oriented output either directly or using its internal block-RAM to the backplane in case of the instructions or the waveform-data, respectively. All outputs of the control-board are galvanic-isolated followed by a signal-current enhancement provided by octal bus transceivers. A configuration programmable read-only memory (CPROM) and a serial electrically erasable programmable read-only memory (EEPROM) are used to auto-configure the FPGA and the USB μC after power-up, respectively. The components of the control-board and the data flow among them are detailed in Fig. 2.

All voltage supplies required by the components on the control-board (1.2 V, 2.5 V, 3.3 V, and 5.0 V) are down-converted on-board from a single +5.0 V supply using DC-DC converters. A galvanic isolated TTL compatible input and output is provided to synchronize operation of the device with rest of the devices in the experiment. The TTL input can be used either as a trigger for internal clock or to apply a signal as an external clock for the synchronized use of the MAWG.

A 24 MHz crystal is used by the USB μC to generate internally 480 MHz and 48 MHz clocks needed for USB data transmission. Furthermore, a 50 MHz on-board oscillator is used by the FPGA to generate clock signals by means of internal frequency divisions, which are needed for the *write* and the *read* operations of the MAWG.

B. The backplane with the daughter-cards

The backplane holds 12 identical daughter-cards such that each daughter-card shares a common data-, control-, and address-bus. The waveform-data received from the control-board are delivered to a daughter-card via the backplane during the *write* operation of a channel on the daughter card. All bus lines are impedance-matched and resistor-terminated on the backplane. Three supply voltages +3.3 V and $\pm$ 12 V (optionally $\pm$ 15 V) generated by a dedicated external power supply are distributed to each daughter-card through the backplane.

All power lines are protected by Zener diodes at the entrance of the backplane.

The daughter-card contains the circuitry to generate two independent voltages. The key components used on the daughter-card along with a flow of data and control signals are
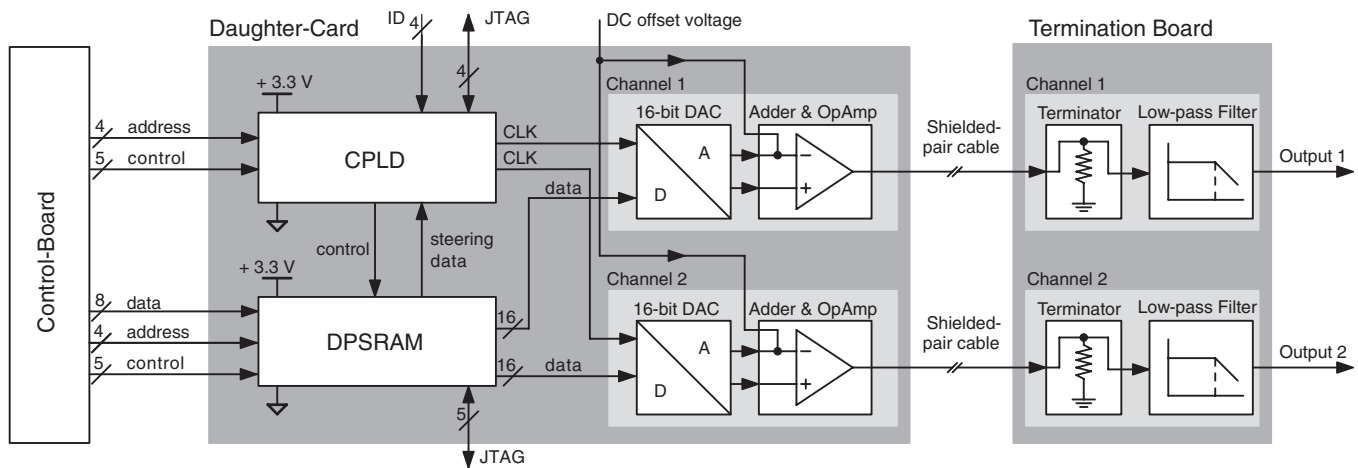
FIG. 3. Block diagram of the daughter-card circuitry. A flow of the digital data and the control signals from the FPGA on the control-board to the CPLD and the DP-SRAM on the daughter-card is laid-out in detail followed by block diagrams of the channels, the termination resistors, and the low-pass filters.

shown in Fig. 3. The CPLD controls signals received by the card and generates clock pulses for the digital-to-analog converter (DAC) along with the control signals to the DP-SRAM on the same daughter-card. The control signals manage storage of the data to a particular address of the DP-SRAM when a *write* operation of the MAWG is executed or deliver the stored data from a particular address of the DP-SRAM to the desired DAC when a *read* operation of the MAWG is performed. The CPLD and the DP-SRAM serve for both channels of the respective daughter-card. Each 16-bit DAC converts respective digital code into a pair of analog signals and delivers it to the operational amplifier (OP-AMP). The output voltages provided by a daughter-card are coupled to a shielded-pair cable with 110 Ω characteristic impedance. The key components of the daughter-card are listed in Table I.

A channel on the daughter-card can be operated in two modes of operation, *stopped-clock* and *continued-clock*. In the *stopped-clock* mode the DAC of the channel holds last value of the voltage sequence being read from the DP-SRAM without getting further clock signal from the CPLD whereas in the *continued-clock* mode the DAC gets a continuous clock

and refreshes the last value of the voltage sequence being read from the memory with the user-defined clock update rate.

C. A channel on the daughter-card

A single channel on a daughter-card consists of a complementary current-type-output 16-bit DAC, followed by a low-noise, high-speed OP-AMP in differential configuration with a gain equal to 10. The DAC converts the user defined voltage code, pre-stored in the DP-SRAM using the *write* operation, into two corresponding analog current signals with a 16 bit resolution. These current signals are then converted into two voltage drops across 50 Ω resistors, referenced to the analog ground (AGND). The voltage drops are finally subtracted and amplified through the OP-AMP circuit. An optional addition of a DC-offset voltage of up to ± 7 V_{pp} is also provided which is common to all channels and can be used to shift the reference level of the final output provided that the sum of amplitudes of the actual and offset voltages does not exceed the output amplitude limits of the channel (see Fig. 4).
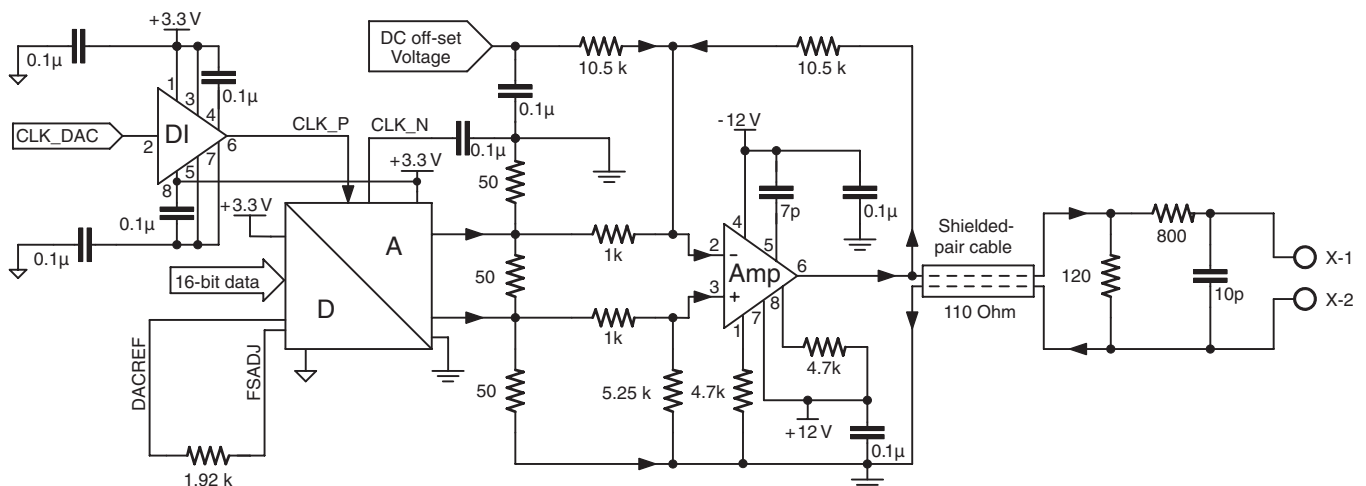

FIG. 4. A detailed circuit diagram for a channel on the daughter-card. The digital signals from the DP-SRAM are converted to the analog signals in the DAC followed by an optional addition of the DC-offset at the differential OP-AMP with an amplification of 10. Downstream the output is terminated and low-pass filtered. The digital isolator provides the noise-free clock signal to the DAC.

The DAC is configured to use the full scale output current amplitude ($\pm$ 20 mA) and to use an internal band-gap reference voltage (1.2 V) provided by the DAC itself. The output of the DAC has a latency of 3.5 clock cycles.

D. The memory management on the daughter-card

The DP-SRAM has a total capacity of 128 k words with a word-width of 36 bits. The DP-SRAM is organized by dividing the full word of the memory into two sub-words of 18 bits each, such that each word serves to hold one data code of a channel on the respective daughter-card by using 16 bits, whereas the remaining 2 bits are reserved for optional steering data. The full depth of the DP-SRAM is divided into 16 logical segments of 8 k words each, which in practice reduces the width of address bus to access the memory from 16 to 4 bits and hence results in a reduced digital noise on the daughter-card at the expense of discrete access to the memory only at start-addresses of the 16 segments.[33]

Each segment of the DP-SRAM can be used to store an individual voltage sequence of up to 8 k words. A voltage sequences larger than the size of the segment can be stored on multiple adjacent segments until the end of the memory. Once a memory segment is accessed at the beginning of the *write* or the *read* operation, the address-control is passed to the DP-SRAM for further increment of the address, using its internal counter, which can be continued across the segments until the end of the memory. Fig. 5 shows details about the memory address management and the bit-assignment of one 36 bits memory word. The waveforms stored on different segments can be retrieved with a switching latency of 4 clock cycles from one segment to another (e.g., 160 ns for 25 MHz update rate). Writing up the data for full depth of the DP-SRAM of a channel needs around 32 ms.

E. Printed circuit boards (PCB)

The PCB for the control-board and the backplane are designed with 4-layers, while the daughter-cards are designed with 6-layers architecture. Routing of the signals is managed on top and bottom layers, whereas the inner layers are

DAC2				DAC1			
35	34 ... 27	26	25 ... 18	17	16 ... 9	8	7 ... 0
bit	MS-Byte	bit	LS-Byte	bit	MS-Byte	bit	LS-Byte

address		
⋮ 8191	segment 2-1	segment 1-1
⋮ 16383	segment 2-2	segment 1-2
⋮ 122879	⋮	⋮
⋮ 131071	segment 2-16	segment 1-16

FIG. 5. Memory management scheme in the DP-SRAM of the daughter-card. Each word of the memory is divided into two sub-words serving for both channels independently while depth of the memory is divided into 16 logical segments. A bit-assignment for one 36 bits memory word is also shown with indication of four reserved bits to be used for steering the data. Each memory segment holds 18 432 bytes.

reserved only for power and ground planes with solid and large copper areas, which ensure a good high-speed performance due to provision of shortest return current path for signals, low thermal resistance for heat dissipation, reduced parasitic inductance, and up to some extent electromagnetic shielding.[34,35]

The partitioning of the digital and the analog ground- and power-planes keeps them separated to make it sure that rich in noise digital circuitry does not affect the performance of the analog part.[34,36–39] On the other hand, the digital and the analog grounds are connected to a single common point with a high impedance resistor to avoid dipole and loop antenna effects due to a difference of potentials and large return path, respectively.[34,35,38]

Routing of the digital and analog signals is done with extensive care, such that not even a single digital signal trace is crossing the analog ground or power plane and vice versa. In addition to the careful routing, the clock signal to the DAC is routed through a galvanic isolator (that bridges analog and digital grounds and power planes) to maintain the current-loop separation strictly. In addition to the general mixed-signal design recommendations, the particular PCB design recommendations for the DAC and OP-AMP are also followed to get optimum performance. In particular, the OP-AMP is ensured to have the shortest feedback connection and ground-free area under the signal input traces to avoid ringing and overshoot, as well as to reduce a stray input capacitance.[35]

F. Power distribution network

The distribution of electrical power for all IC-components is provided to the daughter-card PCB via dedicated inner planes with large surface and hence low impedance. A hierarchical network of decoupling capacitors is implemented to ensure availability of large amounts of current slowly by bulk capacitors as well as less amounts of current rapidly by small capacitors[37,40] required by the components on the control-board and the daughter-card PCBs. A low-pass filter with RF inductance and two capacitances (of 10 μF and 1 μF) in parallel combination are used at each power supply injection into the daughter-card PCB. A decoupling capacitor of 100 nF is placed as close as possible to each power pin of all ICs which decouples the high frequency noise from the analog ICs and work as a charge reservoir for digital ICs to provide the frequently required charge during switching of digital components to avoid the corruption of logic levels.[37]

Towards the superior goal of reducing the noise voltage in the system, we took several layout related practical measures, among them we satisfied the following key recommendations for mixed-signal PCB design:[37,41–46] (1) Selecting ceramic decoupling capacitors with small SMD package and low equivalent series inductance. (2) Placing decoupling capacitors as close as possible to the power pins of the ICs ($\sim$4 mm). (3) Maximizing power-to-ground inter-plane capacitance by minimizing the distance between the power and ground planes ($\sim$0.4 mm). (4) Eliminating unwanted capacitance between digital power- and analog ground-planes (and vice versa) by avoiding their geometrical overlap.
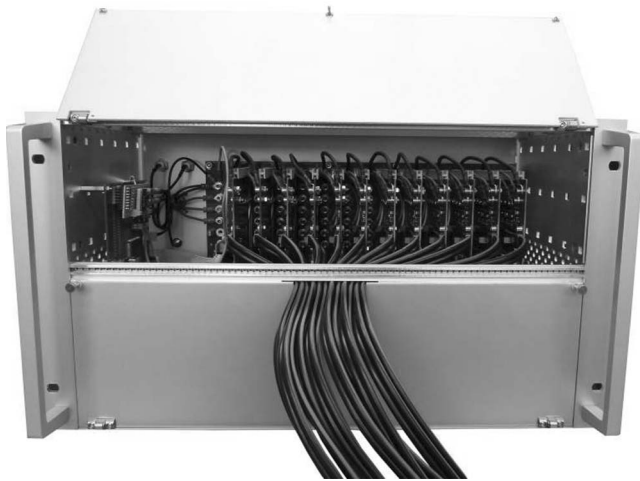
FIG. 6. The MAWG device showing the control-board (on left) and the back-plane housing 12 daughter cards on it.

Since low inductance path from decoupling capacitors to ground plane enhances effectiveness of noise bypassing, its implementation was pursued consequently with high priority during the PCB layout. Based on calculations given in Ref. 46, the above design considerations would result in an expected inductance of about 2 nH per single decoupling capacitor and a power pin of the IC.

Fig. 6 shows the fully assembled MAWG with the control-board (on left side in the box) and 12 daughter cards mounted on the backplane.

III. SOFTWARE ARCHITECTURE

The software needed to run the MAWG was developed in VHDL, C, and LabVIEW. The firmware development for the FPGA and the CPLD was done in VHDL and both of the devices are burned with the tested programs using software interfaces provided by the respective vendors. A high-level user-interface to control the MAWG parameters at the run-time is designed in the C as well as in the LabVIEW programming languages. Both applications provide graphical user interface (GUI) for easy access to the MAWG device. Fig. 7
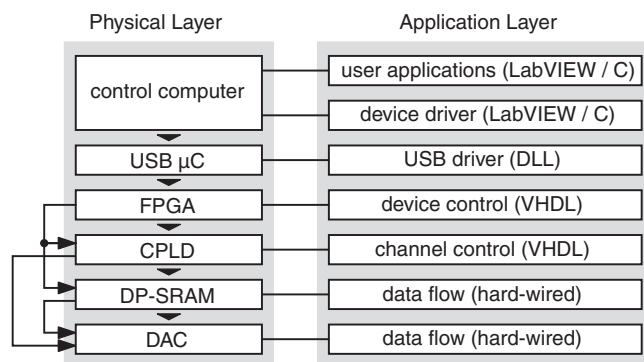

FIG. 7. Software architecture model of the MAWG showing the physical and the application layers along with their inter-connections. The arrows from top to bottom show data flow whereas arrows on left side show flow of control among components of the physical layer.
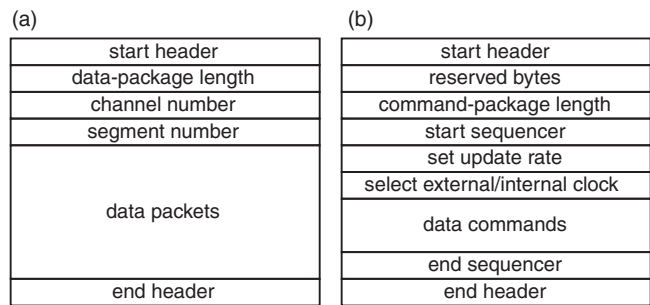

FIG. 8. Protocols defined to send the data-package (a) and the command-package (b) from the control computer to the MAWG.

shows a model-based architecture of the developed software along with the flow of information from one physical- and application-layer component to the other one.

The user communicates with the MAWG device by means of sending data-packages for writing into the DP-SRAM and subsequently command-packages for execution in a command sequencer (CS), designed and implemented inside the FPGA. Both communication packages follow a pre-defined data and command bit-formats.

The data-package protocol (Fig. 8(a)) is used to send the data to be written on the DP-SRAM of a daughter-card. It starts with a start-header followed by information of length of the data-package, the channel number, and the segment number to be written. Then comes the data in form of packets of 9 B each and at last the end-header to stop the process of writing the DP-SRAM.

Similarly, the command-package protocol (Fig. 8(b)) consists of instructions to read a pre-stored data from the DP-SRAM and make it available for the DAC. It starts with a start header followed by the length of the command package and the instruction to start the sequencer which encapsulates a list of commands followed by the instruction to end the sequencer and the header. The list of commands consist of configuration commands followed by a combination of five data-handling commands. The configuration commands, *SetUpdateRate* and *SelectExternalClock*, configure the clock update rate for the internal clock or enable/disable the external clock for the *read* operation of the device, respectively. The data-handling commands, *StartSegment, Pause, Repeat, WaitForPulse,* and *SendPulse*, manipulate the data according to user defined combination of these commands. All data-handling commands have an implicit index starting with 0. An exemplary command sequencer[47] is given in Table II.

IV. PERFORMANCE

A. Generation of arbitrary waveforms

A few exemplary chosen demo-waveform signals generated by the MAWG are displayed in Fig. 9 to demonstrate capability of the MAWG. Fig. 9(a) presents an abrupt change of voltage from the minimum to the maximum accessible value which shows the amplitude span, the large slew rate, and no visible ringing. Fig. 9(b) presents a sequence of small fast voltages steps with 80 ns dwell time demonstrating the large bandwidth. Fig. 9(c) shows the generation of an arbitrary

TABLE II. Exemplary sequence of commands to get the waveform data pre-loaded in the DP-SRAM. The code for the commands consists of command identifier (number on left) and parameter for action (rest of the number/numbers).

Implicit index	Command	Code	Explanation
	StartSequencer	32 : 0	Start execution of the command sequencer.
	SetUpdateRate	34 : 2	Set the update frequency equal to 25 MHz (50 MHz divided by 2).
	ExtCLK_Disable	35 : 0	Enable internal clock for read operation of the MAWG.
0	WaitForPulse	19 : 0	Wait for external trigger to start the sequencer.
1	StartSegment	02 : 7250	Output 7250 words starting from beginning of the segment 2 of the DP-SRAM.
2	Pause	16 : 255	Pause the execution for 255 clock cycles.
3	StartSegment	05 : 10500	Output 10 500 words starting from beginning of the segment 5 of the DP-SRAM.
4	Repeat	17 : 0 : 11	Repeat 11 times the execution of preceding commands starting from index 0.
5	SendPulse	18 : 170	Issue an output pulse for 170 clock cycles for external synchronization.
	EndSequencer	41 : 0	End execution of the command sequencer.

waveforms (here a Bessel function). Fig. 9(d) presents a triangular waveform showing a good linearity of the output.

B. Output voltage range

The low-noise OP-AMP (AD8021) has a linear output current limit of 70 mA which determines the maximum output voltage amplitude depending on the value of the termina-

tion resistor. A resistor value that needs the amount of current larger than the specified current limit of the OP-AMP will cause saturation of the output voltage. On the other hand, for higher bandwidth output a proper impedance matching between the shielded-pair transmission-line (with characteristic impedance of 110 Ω) and the termination resistor value on the end of the line is obligatory to minimize the output-signal distortion due to signal reflections. As depicted in Fig. 10(a)
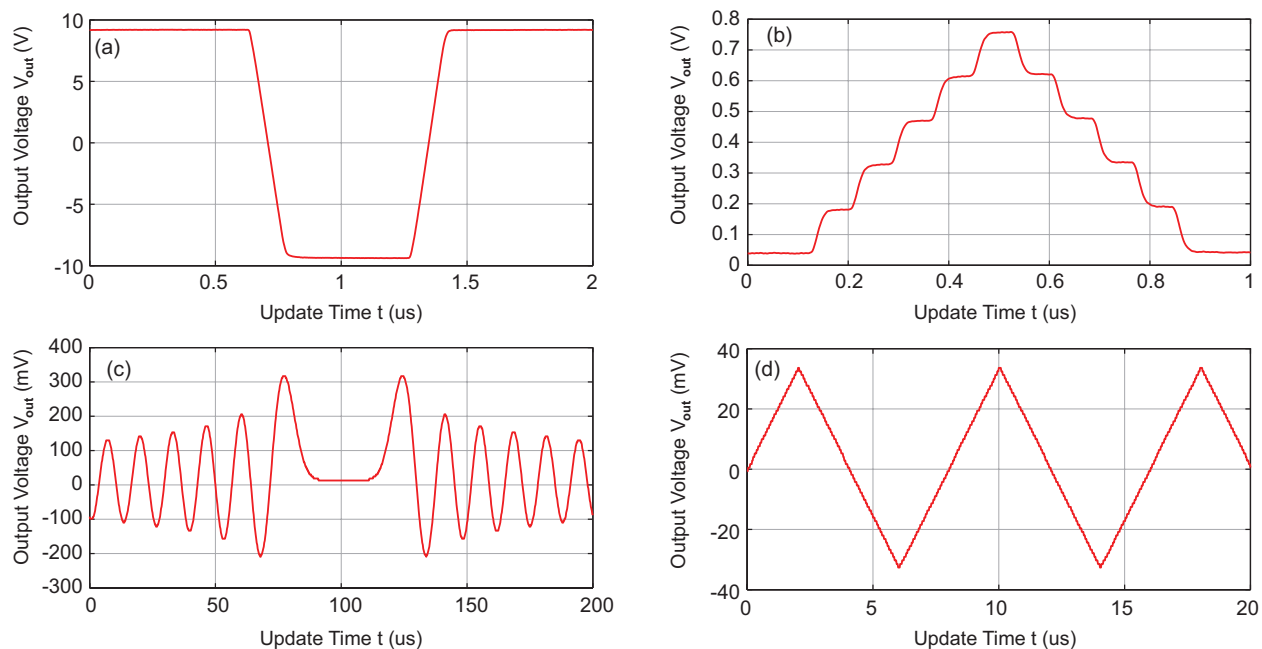

FIG. 9. Versatile waveforms generated by the MAWG: (a) an abrupt changed voltage with a large slew rate, and no visible ringing, (b) a sequence of small fast voltages steps, (c) generation of arbitrary waveforms (here a Bessel function), and (d) a triangular waveform with a good linearity of output.
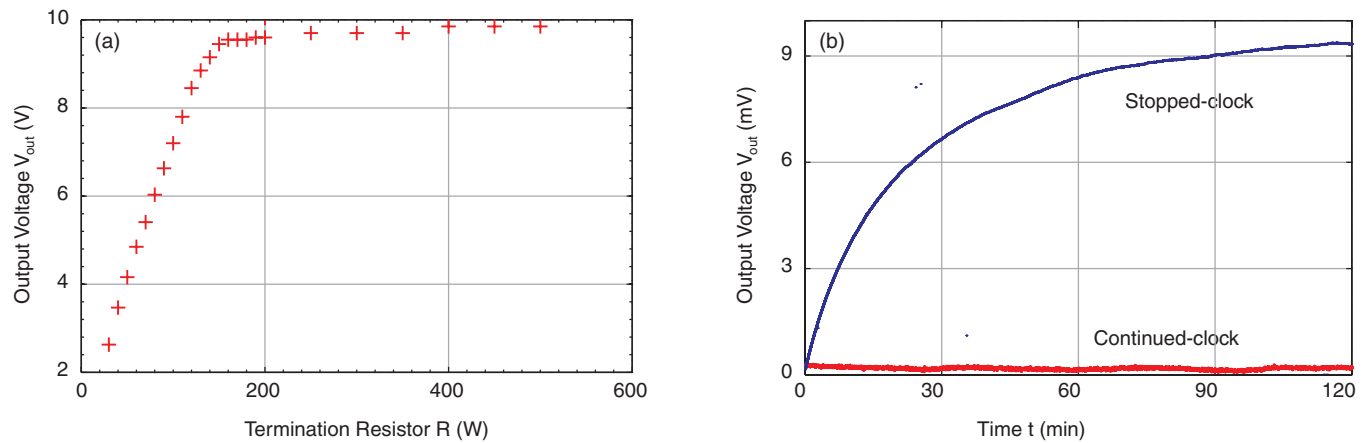
FIG. 10. (a) The output voltage of a channel of the MAWG as a function of termination resistor, showing the saturation of the output voltage after a certain resistor value. (b) Output voltage drift of a channel of the MAWG for the *stopped-clock* and the *continued-clock* modes of operation. The *continued-clock* mode is used with 1 MHz update rate which is the minimum required update rate for the DAC.

the impedance matching scheme with 120 Ω termination resistor provides a maximum signal amplitude range of ± 8.5 V. Though, for low-speed signals of less than 1 Msps, the termination resistor can be increased to 333 Ω, resulting in a less demand for the driving current and consequently providing higher maximum signal amplitude of nearly ± 10 V practically without compromising the signal waveform quality. The measured output impedance of the MAWG channel, determined from Fig. 10(a) at half of the maximum signal amplitude, amounts to 65 Ω.

Another OP-AMP (THS4631D) is tested to provide higher current and hence higher output voltage resulting in maximum output voltages of ± 13 V and ± 11 V for the low- and high-speed signals, respectively, and an output impedance of 45 Ω and a thermal dependence of around 200 μV/$^\circ$C. The OP-AMP is equipped with $\pm$ 15 V supply and configured with a gain of 13.

The characterization of the device and results presented are based on the OP-AMP (AD8021) with a termination resistor of 333 Ω.

C. Output voltage precision

The MAWG device has a linear output signal amplitude behaviour over full range of the operation. A discrepancy between the expected and obtained voltages is found to be below $\pm$ 4 mV with a standard deviation of 0.81 mV (possibly limited by the measurement device). The discrepancies vary randomly among different channels due to manufacturing imperfections of the components and can be compensated by a software calibration of each channel. The main contribution to the output voltage discrepancy is the offset of the output voltage, which results from an intrinsic OP-AMP input-offset-voltage of typically $\pm$ 0.4 mV which results in $\pm$ 4 mV after amplification.

D. Output voltage long-term stability

The MAWG device is characterized by dynamic update rates from 25 Msps down to DC-signal generation. Long-term

stability of DC output signals is of particular interest for applications in quantum information processing. The static operation of the MAWG channel is determined mainly by the performance of our DAC component, which is specified by the vendor for output signal update rates from 1 Msps to 200 Msps.

In the *stopped-clock* mode of operation, the updating of the DAC is suspended during static output voltages, resulting in an idle state of digital switching. This mode reduces the clock noise on the output signal at the expense of a voltage drift of up to several mV for long term operation with some variations among different channels. On the other hand, in the *continued-clock* mode of operation, the DAC is updated continuously with a user-defined clock and hence gives an output voltage with higher stability, however with a tradeoff on noise.

An output signal fluctuating around the set voltage with a maximum deviation less than $\pm$ 150 μV over a period of 2 h and long term drift with a slope below 10 μV/min is observed when the clock is operated with the minimum specified clock update rate of 1 MHz (Fig. 10(b)). A combined operation of both modes can be used to get optimum performance. For example, in a particular experiment, the device can be operated in the *stopped-clock* mode to get the low-noise output during the measurement and then can be switched to the *continued-clock* mode to get the low-drift output during waiting time between two consecutive measurements.

The overall thermal dependence of the MAWG output voltage is around 70 μV/$^\circ$C and is measured by a gradual increase of temperature by up to 14 $^\circ$C starting from the ambient air temperature.

E. Output voltage noise level

The analysis of the MAWG output voltage noise is based on the spectral noise density (SND) ρ of the device measured with the *stopped-clock* mode of operation. The SND of the MAWG is determined for the full range of its output voltages by taking several voltage spectra for different DC output voltages, whereas a wider spectral range from 1 Hz to 200 MHz was covered by using two different spectrum analysers[48] and
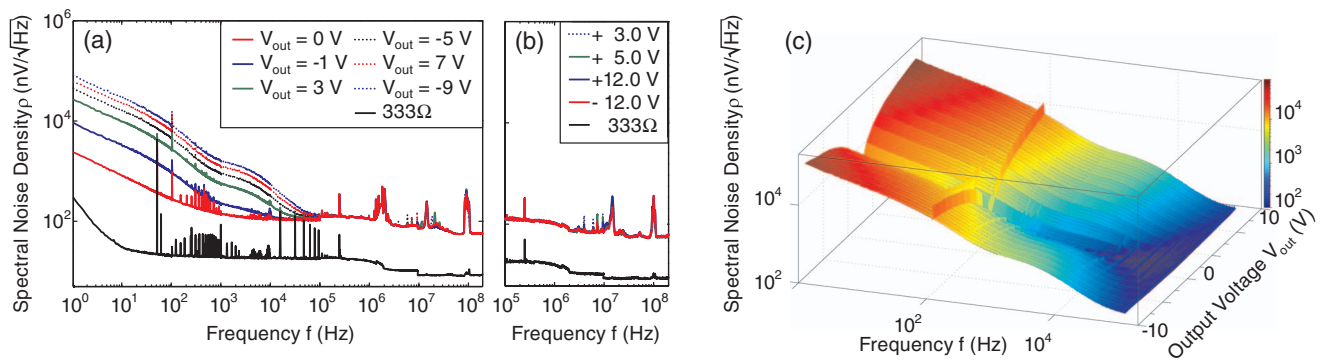
FIG. 11. (a) The spectral noise density measured for the output of one channel of the MAWG, in the *stopped-clock* mode of operation, with the termination resistor but without the low-pass filter. The spectra up to 100 kHz and higher frequencies are taken by two devices with an average of 1000 and 10000, respectively. The black spectrum represents the measurement noise floor obtained by taking the spectra across a naked resistor. (b) The SND measured at the input of the MAWG (i.e., contributions from power supply and pick up from externally generated radio frequencies) explaining the noise peaks at higher frequencies present in the spectral noise density profile at the output of the MAWG. (c) The spectral noise density measured as a function of frequency and output voltages for the frequency range below 100 kHz.

later concatenating the resulting spectra for each of the cases (Fig. 11(a)). The SND spectra are calculated using the relation

$$\rho = \sqrt{\frac{\sigma_v^2}{RBW}},$$

where σ_v is the noise voltage and RBW is the resolution bandwidth of the spectrum analyser for a particular frequency scan.

The SND spectra of the output of a channel of the MAWG, in the *stopped-clock* mode of operation, as a function of the frequency are shown in Fig. 11(a) for a couple of positive and negative output voltages. The spectrum labelled as "333 Ω" is taken using the bare load-resistor and represents noise contributions from the measurement.

The spectra show discrete contributions mainly from 50 Hz and its harmonics in low frequencies. Some additional noise components are visible at frequencies higher than 1 MHz which are identified as a combined effect of power supply output and pick-up of externally generated radio frequencies. The smooth noise floor of the output voltage has a direct dependence on absolute output voltage up to a frequency of 100 kHz whereas for rest of the observed spectrum this dependence is negligible. A measurement for the MAWG input noise density including power supply output and the 2 m long, multi-pole, interconnect cable is plotted in Fig. 11(b)

which explains the peaks present in the spectra at higher frequencies and hence can be avoided by using a storage power supply and/or implementing a proper low-pass filter at output of the MAWG. In the following analysis, contributions appearing above 100 kHz are therefore neglected.

The increasing noise floor with increasing output voltage (Fig. 11(c)) is caused by an asymmetry between two complementary output currents of the DAC (see Sec. II C) which are symmetric for 0 V output and become asymmetric otherwise. The asymmetry increases proportionally to the absolute value of the output voltage. A noise cancellation between complementary outputs occurs in the differential OP-AMP, with a maximum noise reduction for the symmetric case and a lower otherwise. On the other hand, the noise floor for each of the output voltage settings decreases strongly with rising frequency. In Fig. 12(a), the SND is shown as a function of channel output voltage at a couple of frequencies (other than the frequencies corresponding to the 50 Hz harmonics).

The root-mean-square noise v_{rms} of a channel of the MAWG is calculated using the relationship

$$v_{rms} = \sqrt{\sum_{i=1}^{N-1} \langle \rho_{i,i+1}^2 \rangle \triangle f_{i,i+1}},$$
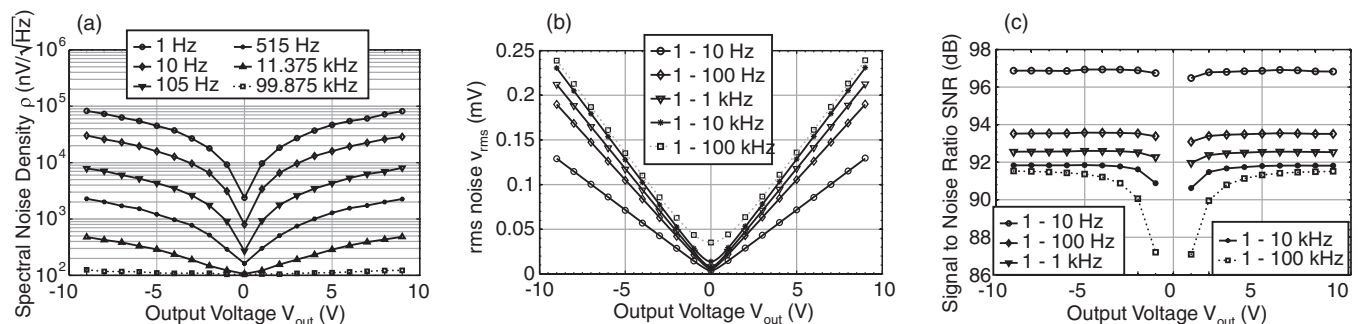

FIG. 12. (a) The spectral noise density as a function of the output voltages measured at different frequencies (avoiding the frequencies corresponding to the 50 Hz harmonics. (b) The rms noise as a function of output voltages measured at some random frequency spans. (c) The signal to noise ratio as a function of output voltages measured at the frequency spans. The plots with dotted line and square markers in (a) and (b) & (c) represents the highest frequency and the highest frequency span, respectively.

where $\triangle f$ is the difference of two consecutive frequencies obtained in the SND measurements.

The output voltage noise v_{rms} as a function of the output voltage (V_{out}) for different frequency spans is plotted in Fig. 12(b) which shows a linearly increased v_{rms} with increase in output voltage amplitude of the MAWG and reaches a maximum level of nearly 250 μV at ± 9 V for the frequency span of 100 kHz. Similarly, an increased frequency span results in a corresponding increase in the root mean square noise which remains consistent for all different output voltages.

The signal to noise ratio (SNR) of the MAWG output is calculated for different output voltages using the relationship

$$ SNR = 10 \cdot \log_{10} \left(\frac{V_{out}}{v_{rms}} \right)^2. $$

The SNR as a function of output voltage V_{out} is plotted in Fig. 12(c) for the same frequency spans. The dependence of the SNR on the output voltage is more pronounced for higher bandwidth whereas for constant bandwidth the dependence is strongest on smaller voltages. The bandwidth of 100 kHz has a SNR greater than 90 dB for the output voltages larger than 2 V.

V. CONCLUSIONS

The MAWG is a general purpose DAC-based system designed to provide multichannel voltage signals characterized by the high dynamic range of both signal amplitude and signal update rate, as well as by a low signal noise and a very good long-term signal stability.

The MAWG is characterized by a large range of signal amplitudes of up to ± 9 V, a wide dynamic range of update rates from 25 Msps down to DC signal generation, as well as a low signal-to-noise ratio of +90 dB and long-time stable output signal amplitude within ± 0.3 mV. The user-control of the device is provided by means of high-level PC-software applications, as well as device firmware, for storing pre-defined voltage sequences and for generating output signals in real time. The overall modular concept of the hardware and embedded software allows for a broad flexibility in various operation schemes and particularly in the performance tuning.

Although the detailed specifications of the device are defined in response to technical challenges of experimental quantum information processing, its practical use for other applications in the fields of fundamental and applied research is easily conceivable, especially in those of similar needs for outstanding instrumentation performance.

ACKNOWLEDGMENTS

[1]J. I. Cirac and P. Zoller, Phys. Rev. Lett. **74**, 4091 (1995).

[2]R. Blatt and D. Wineland, Nature (London) **453**, 1008 (2008).

[3]M. Johanning, A. F. Varon, and C. Wunderlich, J. Phys. B **42**, 154009 (2009).

[4]R. Blatt and C. F. Roos, Nat. Phys. **8**, 277 (2012).

[5]D. Kielpinski, C. Monroe, and D. J. Wineland, Nature (London) **417**, 709 (2002).

[6]S. A. Schulz, U. Poschinger, F. Ziesel, and F. Schmidt-Kaler, New J. Phys. **10**, 045007 (2008).

[7]D. Kaufmann, T. Collath, M. T. Baig, P. Kaufmann, E. Asenwar, M. Johanning, and C. Wunderlich, Appl. Phys. B **107**, 935 (2012).

[8]G. Wilpers, P. See, P. Gill, and A. G. Sinclair, Nat. Nanotechnol. **7**, 572 (2012).

[9]P. J. Kunert, D. Georgen, L. Bogunia, M. T. Baig, M. A. Baggash, M. Johanning, and C. Wunderlich, "A planar ion trap chip with integrated structures for an adjustable magnetic field gradient," Appl. Phys. B (published online).

[10]D. J. Wineland, C. Monroe, W. M. Itano, D. Leibfried, B. E. King, and D. M. Meekhof, J. Res. Natl. Inst. Stand. Technol. **103**, 259 (1998).

[11]M. Rowe, A. Ben-Kish, B. Demarco, D. Leibfried, V. Meyer, J. Beall, J. Britton, J. Hughes, W. Itano, B. Jelenkovic, C. Langer, T. Rosenband, and D. Wineland, Quantum Inf. Comput. **2**, 257 (2002).

[12]A. Walther, F. Ziesel, T. Ruster, S. T. Dawkins, K. Ott, M. Hettrich, K. Singer, F. Schmidt-Kaler, and U. Poschinger, Phys. Rev. Lett. **109**, 080501 (2012).

[13]R. Bowler, J. Gaebler, Y. Lin, T. R. Tan, D. Hanneke, J. D. Jost, J. P. Home, D. Leibfried, and D. J. Wineland, Phys. Rev. Lett. **109**, 080502 (2012).

[14]J. F. Eble, S. Ulm, P. Zahariev, F. Schmidt-Kaler, and K. Singer, J. Opt. Soc. Am. B **27**, A99 (2010).

[15]A. Steane, Rep. Prog. Phys. **61**, 117 (1998).

[16]M. Sasura and V. Buzek, J. Mod. Opt. **49**, 1593 (2002).

[17]R. Raussendorf, D. E. Browne, and H. J. Briegel, Phys. Rev. A **68**, 022312 (2003).

[18]H. Wunderlich, C. Wunderlich, K. Singer, and F. Schmidt-Kaler, Phys. Rev. A **79**, 052324 (2009).

[19]M. Kumph, M. Brownnutt, and R. Blatt, New J. Phys. **13**, 073043 (2011).

[20]R. Schmied, J. H. Wesenberg, and D. Leibfried, Phys. Rev. Lett. **102**, 233002 (2009).

[21]J. W. E. Lybarger, "Enabling coherent control of trapped ions with economical multi-laser frequency stabilization technology," Ph.D. dissertation, University of California, Los Angeles, 2010.

[22]C. Schneider, D. Porras, and T. Schaetz, Rep. Prog. Phys. **75**, 024401 (2012).

[23]C. Wunderlich and C. Balzer, Adv. At., Mol., Opt. Phys. **49**, 293 (2003).

[24]A. Khromova, C. Piltz, B. Scharfenberger, T. F. Gloger, M. Johanning, A. F. Varón, and C. Wunderlich, Phys. Rev. Lett. **108**, 220502 (2012).

[25]A. J. DeMaria and D. A. Stetser, Appl. Phys. Lett. **7**, 71 (1965).

[26]A. Jolly and P. Estraillier, Opt. Laser Technol. **36**, 75 (2004).

[27]S. A. Serati, G. D. Sharp, R. A. Serati, D. J. McKnight, and J. E. Stockley, Proc. SPIE **2490**, 378–387 (1995).

[28]A. M. Weiner, Rev. Sci. Instrum. **71**, 1929 (2000).

[29]R. Grimm, M. Weidemüller, and Y. B. Ovchinnikov, Adv. At., Mol., Opt. Phys. **42**, 95 (2000).

[30]R. Folman, P. Krüger, J. Schmiedmayer, J. Denschlag, and C. Henkel, Adv. At., Mol., Opt. Phys. **48**, 263 (2002).

[31]M. T. Baig, M. Johanning, A. Wiese, M. Ziolkowski, and C. Wunderlich, German Patent DE 10 2011 001 399 A1 (20.09.2012).

[32]All devices and components listed are specified for traceability purpose only and are not mentioned for advertising them, nor do we claim superior performance.

[33]M. T. Baig, M. Ziolkowski, M. Johanning, and C. Wunderlich, Verhandl. DPG (VI) **45**, 1/A 23.50 (2010).

[34]H. W. Ott, Printed Circuit Des. **18**, 8 (2001).

[35]J. Ardizzoni, Analog Dial. **39**, 3 (2005).

[36]H. W. Johnson and M. Graham, *High-Speed Digital Design: A Handbook of Black Magic* (Prentice Hall PTR, Englewood Cliffs, NJ, 1993), Chap. 5.

37 *Op Amps for Everyone: Design Reference*, edited by R. Mancini (Texas Instruments, 2002), Chap. 17.

38 S. Rizvi and I. Khan, Printed Circuit Des. Manuf. **22**, 24 (2005).

39 B. Hu and K. Y. See, in *Proceedings of the 7th Electronic Packaging Technology Conference, 2005, EPTC 2005* (IEEE, 2005), Vol. 1, pp. 34–37.

40 J. L. Knighten, B. Archambeault, J. Fan, G. Selli, S. Connor, and J. L. Drewniak, IEEE EMC Soc. Newsl. **207**, 46 (2005).

41 L. Smith, R. Anderson, D. Forehand, T. Pelc, and T. Roy, IEEE Trans. Adv. Packag. **22**, 284 (1999).

42 W. Kester, *Mixed-Signal and DSP Design Techniques* (Analog Devices, Inc., USA, 2000), Chap. 10.

43 J. Fan, W. Cui, J. Drewniak, T. Van Doren, and J. Knighten, IEEE Trans. Adv. Packag. **25**, 154 (2002).

44 B. Archambeault, Printed Circuit Des. Manuf. **24**, 16–17 (2007).

45 B. Archambeault, M. Cocchini, G. Selli, J. Fan, J. Knighten, S. Connor, A. Orlandi, and J. Drewniak, in *Proceedings of the International Symposium on Electromagnetic Compatibility – EMC Europe, 2008* (IEEE, 2008), pp. 1–6.

46 B. Archambeault, IEEE EMC Soc. Newsl. **221**, 71 (2009).

47 Further details about the commands to communicate with the device can be provided by the authors on request.

48 Advantest (R9211B) and Rohde & Schwarz (FSP 30).